Progress In Electromagnetics Research C, Vol. 121, 197–206, 2022

Computational Approach of Designing Magnetfree Nonreciprocal Metamaterial

Swadesh Poddar[1, *], Md. Tanvir Hasan, and Ragib Shakil Rafi

Abstract—This article aims at discussing a computational approach to designing magnet-free nonreciprocal metamaterial. Detailed mathematical derivation on Floquet mode analysis is presented for Faraday and Kerr rotation. Non-reciprocity in the designed metasurface is achieved in the presence of a biased transistor loaded in the gap of circular ring resonator. Based on the derived mathematical model, co- and cross-polarized components have been extracted, which helps find Faraday and Kerr rotation and compare/contrast the reciprocal and nonreciprocal systems.

1. INTRODUCTION

A system is reciprocal when signal transmission between two ports is independent of the propagation direction. Signal transmission between transmitter and receiver can be represented in terms of scattering (S) parameter as $S^T = S$). In our daily life application such as antenna, passive electrical circuits, and components are reciprocal. Nonreciprocal systems, opposite to reciprocal, exhibit different received-transmitted field ratios when the source and observation points interchange. Non-reciprocal components such as circulators, isolators, and gyrators play a pivotal role in many microwave wireless applications, including high-power transmitters, FDD system, emerging quantum computing and readout, defense, and satellite communication, to name a few [2, 11].

A significant amount of research on nonreciprocity has been conducted since 1950 with several proposed approaches using permanent magnets, nonreciprocal components, time modulation parametric amplifiers, etc. [5, 10, 11, 20]. Advancement in solid-state technology and fabricating artificially engineered material, also known as metamaterial, familiar to induce customized nonexistent properties in a material, initiated a research direction in achieving magnet less nonreciprocity via braking time-reversal symmetry. Over the past decade, research into metamaterials has been extended to the search for real-world applications, leading to the concept of meta-devices, defined as metamaterial-based devices that can operate in an active manner [21]. This article primarily aims at the computational approach of designing nonreciprocal metamaterial leading to the practical realization of simulated and machine learning-based optimization. The proposed design in this article is an extension of the transistor-based design first proposed by Kodera et al. [6, 9] followed by our previous articles, "Design and Analysis of an Electronically Tunable Magnet-Free Non-Reciprocal Metamaterial," published in *IEEE Transactions on Antennas and Propagation*, a nonreciprocal metasurface with precise electronic tunability features [15].

The paper's organization follows the insight into the mechanism of Floquet mode analysis and corresponding analytical approach, the principle of ferromagnetic resonance next, later the design approaches and process flow of our nonreciprocal devices, and finally, results and discussion on simulated performance, benchmarking reciprocal, and nonreciprocal design, and highlighting significant challenges, limitations, and future works.

Received 22 May 2022, Accepted 1 July 2022, Scheduled 21 July 2022
* Corresponding author: Swadesh Poddar (poddarswadesh@gmail.com).
[1] Design Engineer, Qorvo US, Inc.

2. FLOQUET MODE ANALYSIS AND MATHEMATICAL MODELING

Based on Floquet mode analysis, this section presents a mathematical model to characterize the unit cell of our designed metasurface. The Floquet port is used with planar-periodic structures. Analyzing a unit cell leads to the analysis of the overall periodic structure, where we used "master and slave" boundaries to model a unit cell of the repeating structure. The fields on the slave surface have constraints identical to that on the master surface, with a phase shift. A coordinate system must be identified on the master and slave boundary to identify point-to-point correspondence, and master and slave surfaces must be of identical shapes and sizes. A set of modes called Floquet modes represent the fields on the port boundary. Fundamentally, Floquet modes are analogous to plane waves, where the frequency and geometry of periodic structures set the propagation direction. To simplify the discussion, we developed a 3D structure and considered 1st two modes to propagate through the metamaterial unit cell with an accordingly designed z-direction Floquet boundary.

Figure 1 shows the proposed metamaterial unit cell in the Floquet port environment. a_{mn} and b_{mn} are the incident wave from the Floquet port 1 and Floquet port 2, respectively. On the other hand, c_{mn} and d_{mn} are the scattered wave. In a normal incidence case where the 1st 2 modes, namely TE and TM, are evaluated and can be expressed in S matrix. In Ansys HFSS simulation, Floquet mode has been analyzed where transverse electric (TE) modes are y polarized, and transverse magnetic (TM) modes are x polarized.

$$\begin{bmatrix} \mathbf{c}_{mn}^{TE} \\ \mathbf{c}_{mn}^{TM} \\ \mathbf{d}_{mn}^{TE} \\ \mathbf{d}_{mn}^{TM} \end{bmatrix} = \begin{bmatrix} \mathbf{S}_{11}^{TE,TE} & \mathbf{S}_{11}^{TE,TM} & \mathbf{S}_{12}^{TE,TE} & \mathbf{S}_{12}^{TE,TM} \\ \mathbf{S}_{11}^{TM,TE} & \mathbf{S}_{11}^{TM,TM} & \mathbf{S}_{12}^{TM,TE} & \mathbf{S}_{12}^{TM,TM} \\ \mathbf{S}_{21}^{TE,TE} & \mathbf{S}_{21}^{TE,TM} & \mathbf{S}_{22}^{TE,TE} & \mathbf{S}_{22}^{TE,TM} \\ \mathbf{S}_{21}^{TM,TE} & \mathbf{S}_{21}^{TM,TM} & \mathbf{S}_{22}^{TM,TE} & \mathbf{S}_{22}^{TM,TM} \end{bmatrix} \begin{bmatrix} \mathbf{a}_{mn}^{TE} \\ \mathbf{a}_{mn}^{TM} \\ \mathbf{b}_{mn}^{TE} \\ \mathbf{b}_{mn}^{TM} \end{bmatrix}, \tag{1}$$

where $\mathbf{c}_{mn}^{TE}$ and $\mathbf{a}_{mn}^{TE}$ define the scattered and incident fields, respectively. Besides, $\mathbf{S}_{ij}^{pol1,pol2}$, where i (pol1) and j (pol2) represent incident and received port (polarization), respectively. For example, $\mathbf{S}_{11}^{TE,TE}$ is the co-polarized reflection case, or in other words incident wave is $TE(y)$ polarized from port 1 and received wave $TE(y)$ polarized to port 1. Similarly, $\mathbf{S}_{21}^{TM,TE}$ defines a cross-polarization transmission case. The above Eq. (1) can be written in a short form as below in terms of Floquet

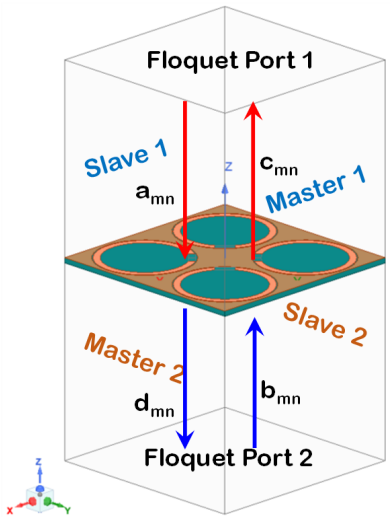

Figure 1. Geometry of proposed metamaterial unit cell. Primary and secondary master and slave boundaries form the side walls of unit cell. In both ports Floquet environment scattered and incident wave is shown with arrow direction.

modes.

$$\begin{bmatrix} \mathbf{c}_{mn}^{TE} \\ \mathbf{c}_{mn}^{TM} \\ \mathbf{d}_{mn}^{TE} \\ \mathbf{d}_{mn}^{TM} \end{bmatrix} = [\mathbf{S}] \cdot \begin{bmatrix} \mathbf{a}_{mn}^{TE} \\ \mathbf{a}_{mn}^{TM} \\ \mathbf{b}_{mn}^{TE} \\ \mathbf{b}_{mn}^{TM} \end{bmatrix}, \tag{2}$$

where

$$\mathbf{S} = \begin{bmatrix} S(\text{FP1}:1,\text{FP1}:1) & S(\text{FP1}:1,\text{FP1}:2) & S(\text{FP1}:1,\text{FP2}:1) & S(\text{FP1}:1,\text{FP2}:2) \\ S(\text{FP1}:2,\text{FP1}:1) & S(\text{FP1}:2,\text{FP1}:2) & S(\text{FP1}:2,\text{FP2}:1) & S(\text{FP1}:2,\text{FP2}:2) \\ S(\text{FP2}:1,\text{FP1}:1) & S(\text{FP2}:1,\text{FP1}:2) & S(\text{FP2}:1,\text{FP2}:1) & S(\text{FP2}:1,\text{FP2}:2) \\ S(\text{FP2}:2,\text{FP1}:1) & S(\text{FP2}:2,\text{FP1}:2) & S(\text{FP2}:2,\text{FP2}:1) & S(\text{FP2}:2,\text{FP2}:2) \end{bmatrix} \tag{3}$$

where FP is the short form of Floquet port used here in Eq. (3). In summary, FP $p:u$, FP $q:u$ means S_{pq} for u polarized as incident and received waves define co-polarization. Similarly, FP $p:v$, FP $q:u$ means S_{pq} for incident mode as u and received wave as v polarized. In this explanation, p and q were used to mention port number and v and u to mention polarization type.

$$\begin{bmatrix} \mathbf{c}_{mn}^{TE} \\ \mathbf{c}_{mn}^{TM} \\ \mathbf{d}_{mn}^{TE} \\ \mathbf{d}_{mn}^{TM} \end{bmatrix} = \begin{bmatrix} \mathbf{R}_{yy}^{(1)} & \mathbf{R}_{yx}^{(1)} & \mathbf{T}_{yy}^{(2)} & \mathbf{T}_{yx}^{(2)} \\ \mathbf{R}_{xy}^{(1)} & \mathbf{R}_{xx}^{(1)} & \mathbf{T}_{xy}^{(2)} & \mathbf{T}_{xx}^{(2)} \\ \mathbf{T}_{yy}^{(1)} & \mathbf{T}_{yx}^{(1)} & \mathbf{R}_{yy}^{(2)} & \mathbf{R}_{yx}^{(2)} \\ \mathbf{T}_{xy}^{(1)} & \mathbf{T}_{xx}^{(1)} & \mathbf{R}_{xy}^{(2)} & \mathbf{R}_{xx}^{(2)} \end{bmatrix} \begin{bmatrix} \mathbf{a}_{mn}^{TE} \\ \mathbf{a}_{mn}^{TM} \\ \mathbf{b}_{mn}^{TE} \\ \mathbf{b}_{mn}^{TM} \end{bmatrix} \tag{4}$$

Equation (4) represents Eq. (1) regarding reflection and transmission for an easier understanding of the Floquet mode analysis, whereas for the R/T matrix, superscript describes the received port number; subscript describes the polarization, e.g., T_{xx}^{1} equals the wave being propagated from port 2 and received at port 1; for generalized understanding, this is analogous to S_{12}. Generally, the reflected and transmitted fields consist of both x- and y-polarized components. The ratio of the transmitted field with polarization x to the incident field with polarization y defines transmission field T_{xy}. Based on the same concept, the ratio of the reflected field with polarization x to the incident field with polarization y represents reflected field R_{xy}.

The incident and transmitted fields are related through Jones transmission matrix in cartesian basis as below [14]

$$\mathbf{T} = \begin{bmatrix} \mathbf{T}_{xx} & \mathbf{T}_{xy} \\ \mathbf{T}_{yx} & \mathbf{T}_{yy} \end{bmatrix} \tag{5}$$

The transmission matrix in linear basis can be mapped to transmission matrix in circular basis as below

$$\mathbf{T}_{CP} = \begin{bmatrix} \mathbf{T}_{\circlearrowright\circlearrowright} & \mathbf{T}_{\circlearrowright\circlearrowleft} \\ \mathbf{T}_{\circlearrowleft\circlearrowright} & \mathbf{T}_{\circlearrowleft\circlearrowleft} \end{bmatrix} = \frac{1}{2}[\mathbf{L}] \tag{6}$$

$$\mathbf{T}_{CP} = \begin{bmatrix} \mathbf{T}_{\circlearrowright\circlearrowright} & \mathbf{T}_{\circlearrowright\circlearrowleft} \\ \mathbf{T}_{\circlearrowleft\circlearrowright} & \mathbf{T}_{\circlearrowleft\circlearrowleft} \end{bmatrix} = \frac{1}{2}[\mathbf{L}] = \frac{1}{2}\begin{bmatrix} T_{xx}+T_{yy}+i(T_{xy}-T_{yx}) & T_{xx}-T_{yy}-i(T_{xy}+T_{yx}) \\ T_{xx}-T_{yy}+i(T_{xy}+T_{yx}) & T_{xx}+T_{yy}-i(T_{xy}-T_{yx}) \end{bmatrix} \tag{7}$$

Based on our above discussion, $\mathbf{T}$ matrix in circular basis can be generalized as below

$$\mathbf{T}_{\circlearrowright\circlearrowright} = \text{Incident RHCP to recieved RHCP} \tag{8}$$

$$\mathbf{T}_{\circlearrowleft\circlearrowright} = \text{Incident LHCP to recieved RHCP} \tag{9}$$

$$\mathbf{T}_{\circlearrowright\circlearrowleft} = \text{Incident RHCP to recieved LHCP} \tag{10}$$

$$\mathbf{T}_{\circlearrowleft\circlearrowleft} = \text{Incident LHCP to recieved LHCP} \tag{11}$$

where RHCP/LHCP stands for right/left handed circular polarization. Once the transmission matrix in circular or linear basis is achieved, Faraday rotation and ellipticity can be calculated from there. Ellipticity, δ_F, is a measure of the polarization state of an electromagnetic wave, and it varies from $+1$ to -1. In terms of RHCP and LHCP, this can be written as

$$\delta_F = \frac{|\,T_{\circlearrowright\circlearrowright}\,| - |\,T_{\circlearrowleft\circlearrowleft}\,|}{|\,T_{\circlearrowright\circlearrowright}\,| + |\,T_{\circlearrowleft\circlearrowleft}\,|} \tag{12}$$

Therefore, from above equation, if $\delta_F = +1$, wave is RHCP, and if $\delta_F = -1$, the wave is LHCP, whereas $\delta_F = 0$ means linear polarized wave.

Faraday rotation can be calculated from the equation below [13]

$$\theta_F = \frac{1}{2}\tan^{-1}\left(\frac{T_{\circlearrowleft\circlearrowleft}}{T_{\circlearrowright\circlearrowright}}\right) \tag{13}$$

Similarly, for a reflection based metasurface, ellipticity and Kerr rotation can be calculated following the same steps as described above.

$$\delta_K = \frac{\mid R_{\circlearrowleft\circlearrowleft}\mid - \mid R_{\circlearrowright\circlearrowright}\mid}{\mid R_{\circlearrowleft\circlearrowleft}\mid + \mid R_{\circlearrowright\circlearrowright}\mid} \tag{14}$$

$$\theta_K = \frac{1}{2}\tan^{-1}\left(\frac{R_{\circlearrowleft\circlearrowleft}}{R_{\circlearrowright\circlearrowright}}\right) \tag{15}$$

3. FERROMAGNETIC RESONANCE

The concept related to the motion of the magnetic dipole in the presence of the magnetic field and a self-consistent RF magnetic field represents the principle idea of ferromagnetic resonance [13]. Microwave magnetism in a ferrite material is based on the precession of the magnetic dipole moments which arise from unpaired electron spins along the axis of an externally applied static magnetic bias. For resonance condition, it is necessary to apply the RF magnetic field (the microwave field) perpendicular to the dc field. The quantum mechanical phenomena can be described from Landau-Lifshitz-Gilbert equation as [12, 13, 15]

$$\frac{d\mathbf{M}}{dt} = \gamma(\mathbf{M}\times\mathbf{H}) - \frac{\alpha}{|M|}\mathbf{M}\times\frac{d\mathbf{M}}{dt}, \tag{16}$$

where α is the Gilbert damping term; γ is the gyromagnetic ratio; $\mathbf{M} = \mathbf{i}_z M_0 + \mathbf{m}e^{j\omega t}$ and $\mathbf{H} = \mathbf{i}_z H_i + \mathbf{h}e^{j\omega t}$, where $\mathbf{i}_z$ is the unit vector in the z direction; $\mathbf{m}$ and $\mathbf{h}$ are RF quantities; and H_i is the total internal dc magnetic field as shown in Fig. 2. The nearer the frequency of the microwave field to the natural precession frequency is, the greater the energy absorbed by the spins will be [13]. The longitudinal (z) component does not contribute to precession and therefore, to magnetism. Since $\mathbf{H}_0 \parallel \widehat{\mathbf{z}}$, the z-component of $\mathbf{M}$ produced by $\mathbf{H}_t^{RF}$ would lead to $[M_z^{RF}(\mu_0 H + H^{RF})](\widehat{\mathbf{z}}\times\widehat{\mathbf{z}}) = 0$. Therefore, the only torque produced by the transverse component at x-y plane can be stated as $(M_t^{RF}\mu_0 H)(\widehat{\mathbf{t}}\times\widehat{\mathbf{z}}) \neq 0$.

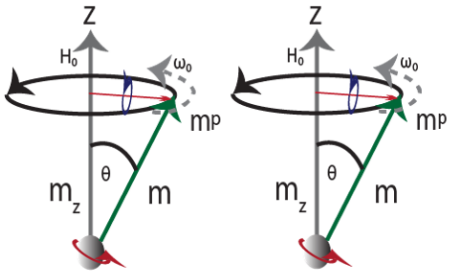

Figure 2. Magnetic dipole precession, arising from electron spinning in a ferrite material about the z axis of an externally applied static magnetic bias field, H_0, with effective unidirectional current loops around z axis and magnetic dipole moment m_ρ.

The magnetization vector described above has a singularity, when $\omega = \omega_0 = \gamma H_0$, which can be defined as the resonance condition. Resonance can be achieved by varying the operating frequency or the applied field until the precession frequency equals the microwave frequency. Permeability tensor of ferrite material can be represented as [17]

$$\overrightarrow{\mu} = \mu_0 \begin{bmatrix} \mu & -jk & 0 \\ jk & \mu & 0 \\ 0 & 0 & 1 \end{bmatrix}, \tag{17}$$

where $\mu = 1 + \frac{\omega_0\omega_M}{\omega_0^2-\omega^2}$, $jk = \frac{j\omega\omega_M}{\omega_0^2-\omega^2}$, and $\omega_M = \gamma 4\pi M_0$.

4. NONRECIPROCAL DEVICE DESIGN

Active devices have been used in the design of magnet-free non-reciprocal metamaterials. For example, a transistor amplifier can be viewed as an isolator that amplifies the input signal in one direction and blocks it in the reverse direction and is very popular in RF microwave devices, metamaterial and antenna design [16, 18, 19]. In a series of publications between 2011 and 2019, Kodera et al. explored the unidirectional properties of transistors in the design of non-reciprocal metamaterials [7–10]. A ring resonator supports two counter-propagating modes with the same resonance frequency, a result of reciprocity. However, when a unidirectional component such as transistor is used in the ring gap, one of the modes is blocked and the ring loaded with a transistor resonates only for one type of circularly polarized wave [11]. A linearly polarized wave can be represented as a sum of RHCP and LHCP waves. When this RHCP and LHCP waves propagate through a material with different phase-velocities, the plane of polarization of the resultant linearly polarized wave rotates. This process of polarization rotation can be reciprocal (e.g., in chiral materials that exhibit a reciprocal magnetoelectric coupling), and it can also be non-reciprocal. In the case of Faraday rotation, the sign of rotation (i.e., clockwise or counterclockwise) is determined relative to the axis along which time-reversal (TR) symmetry is broken (e.g., in a magnetized ferrite, this axis would point parallel to the magnetization direction), whereas in chiral media exhibiting reciprocal magneto-electric coupling, the sign of rotation is determined relative to the propagation direction. For the designing mechanism of metamaterial considered in this work, it is confirmed from that the wave propagation supported by the metamaterial is non-reciprocal, with Faraday rotation being the driving mechanism [15].

Figure 3 shows the travelling wave resonance of a slot ring resonator loaded with transistor and passive components mimicking the electron spin precession in a biased ferromagnetic material. The electrical length (λ) of the ring resonator should be 2π due to phase matching. The wave is traveling

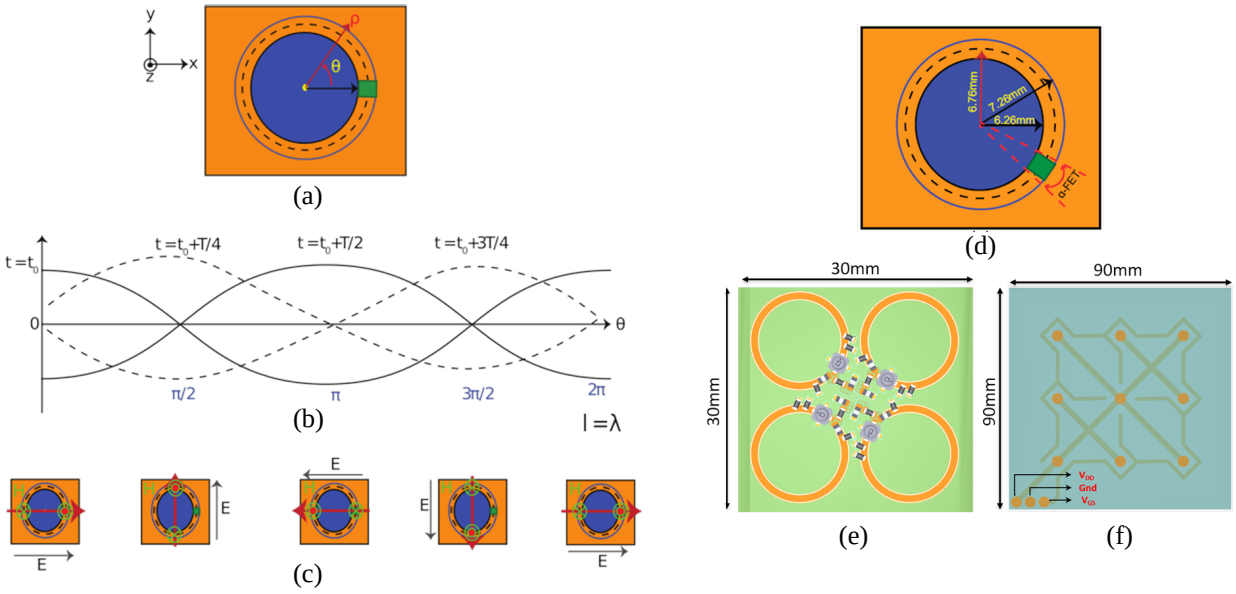

Figure 3. Non-reciprocal gyrotropy. Rotating dipole moment in (a) the proposed metamaterial structure consisting of slot-ring resonator loaded with active components (transistor). (b) Travelling wave along the ring at four quarter-period spaced time instants. (c) Rotating electric field in the slot-ring and the corresponding electric dipole moment due to vectorial magnetic field pointed outward and inward. (d) Dimensions of the ring resonator. (e) Unit super-cell of a 3 by 3 super-cell board consisting of 4 rings in a 90°-symmetric configuration (Top view) to increase the coupling strength [1, 3, 4]. (f) Bias connection layout of the complete board (Bottom view) [15].

(as opposed to a standing wave) due to the presence of the unilateral (transistor) element. Based on the applied electric bias to the active component, the electric dipole moment (red arrow) rotates along the circular ring at four-quarter period spaced time instants. The direction of the electric field follows the direction of the dipole moment. Therefore, non-reciprocal gyrotropy is established in the slot-ring resonator. The circular ring resonates when the electrical length is equal to an integer multiple of 2π.

$$\beta l + \alpha_{FET} = 2m\pi, \tag{18}$$

where β is the propagation constant defined by $\frac{2\pi}{\lambda_g}$; α_{FET} is the physical distance of the ring gap as shown in Fig. 3(d); and l is the physical length of the slotted transmission line defined as $l = (2\pi - \alpha_{FET})r_{mean}$. In this research work, FR4 ($\varepsilon_r = 4.4$) substrate has been used with a thickness of 0.8 mm. The major focus in this research work is the Faraday rotation, an important key performance indicator to quantify nonreciprocity, which is obtained based on the transmission properties. Ground plane has been designed on geometry of the same front side, so the wave can propagate through the metasurface itself. Detailed design modelling has been discussed in our previous work mentioned in the introduction section.

The effective dielectric constant for a microstrip geometry is

$$\varepsilon_e = \frac{\varepsilon_r + 1}{2} + \frac{\varepsilon_r - 1}{2}\left\{1 + 12\left(\frac{H}{W}\right)\right\}^{-\frac{1}{2}}, \tag{19}$$

where Eq. (19) follows the condition $\frac{W}{H} \geq 1$, and Z_0 can be calculated as

$$Z_0 = \frac{120\pi}{\sqrt{\varepsilon_e}\left[\frac{W}{H} + 1.393 + \frac{2}{3}\ln\left(\frac{W}{H} + 1.444\right)\right]}. \tag{20}$$

Based on the above analysis, initial parameters have been calculated considering a resonance frequency at 5.7 GHz and dielectric properties of the FR4 substrate.

Figure 4(a) shows the simulated performance of a ring resonator in a reciprocal condition, i.e., without any active component connected. Based on our previous analysis, nonreciprocal properties cannot be achieved as shown in Fig. 4(b), hence, no Faraday or Kerr rotation. Propagating wave exhibits a linear polarization which can be shown from ellipticity. Figs. 4(c) and (d) show reflection and transmission behavior in terms of scattering parameter. One important observation for the reciprocal device is that the co- and cross-pol components will be in line with each other. For example, we observe no difference between cross-pol reflection parameter, S_{11}^{xy} and S_{11}^{yx}. The co- and cross-pol transmission parameters follow a similar pattern.

Figure 5 shows the setup of the co-simulation. We solved the 3D electromagnetic structure of the metasurface in Ansys HFSS, a passive solver. Besides, the circuit model has been solved independently in a specific bias condition. Later the S parameters are connected using the dynamic link to run the co-simulation and optimization.

Figure 6 shows the process-flow of design and optimization. The operation frequency and preferred dielectric material are selected in the first step. After that, the initial dimension has been calculated based on microwave equation discussed earlier in the section. All dimensions are used as variables for later optimization and sensitivity analysis. Lumped ports are used in the gap, and Floquet based S matrix has been solved for the metasurface. For co-simulation, we cascaded the S parameter from our designed circuit and then solved one from the 3D model in the circuit solver. Once we obtain the initial design and result, based on the targeted goal and machine learning optimization, algorithm design is optimized to achieve nonreciprocity at desired resonance, and the Quasi-newton algorithm from HFSS is used. An in-house script was developed and used during the optimization to calculate and optimize the performance at resonance on key performance indicators such as Faraday, Kerr rotation, and co-cross polarized components.

5. RESULTS AND DISCUSSION

This section will discuss the simulation results of the nonreciprocal metasurface. From region 1, the x-polarized wave transmits from antenna 1 to antenna 2, and the y-polarized probe (antenna) picks

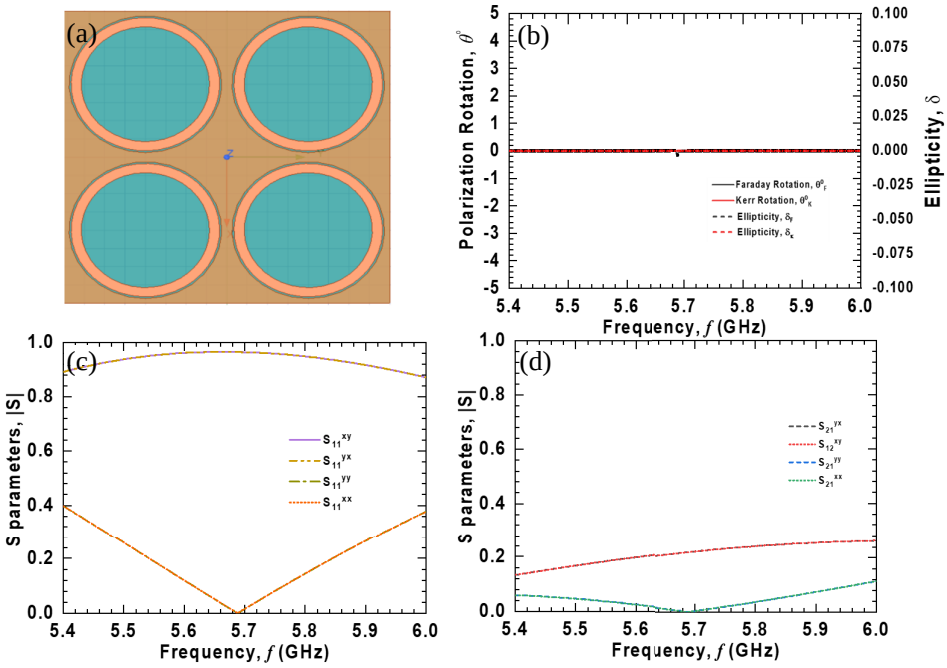

Figure 4. Simulated performance of ring resonator based metamaterial. (a) Simple circular ring resonator based unit cell on proposed metasurface design. (b) The design is reciprocal, hence, no nonreciprocal properties can be observed. (c) Both co pol and (d) cross pol components exhibit the reciprocal behaviour, resonance is observed at 5.69 GHz in this design.

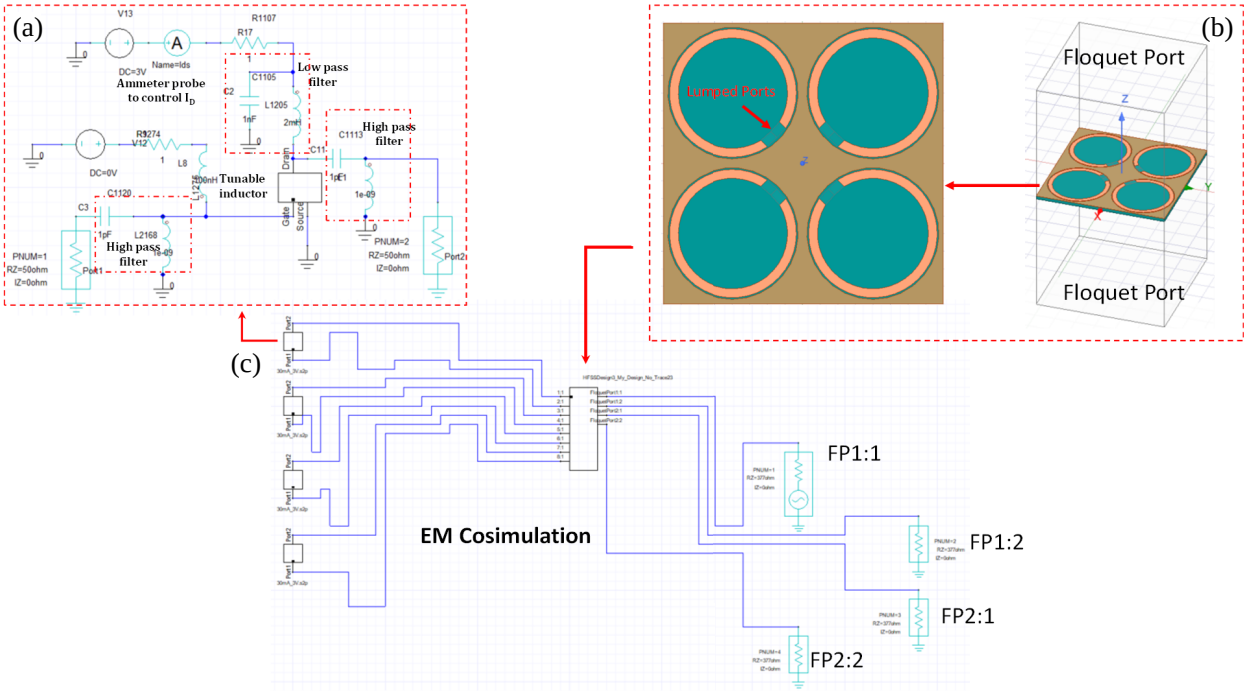

Figure 5. Electromagnetic co-simulation. (a) Circuit configuration that was used to achieve nonreciprocity, nonreciprocal component such as transistor was used to bridge the ring resonator gap, other component are for impedance matching and biasing the transistor in various condition. (b) 3D electromagnetic model of the metamaterial using Floquet mode analysis. (c) S parameter file of the 3D model and circuit model has been connected using dynamic link and to evaluate co-simulation results.

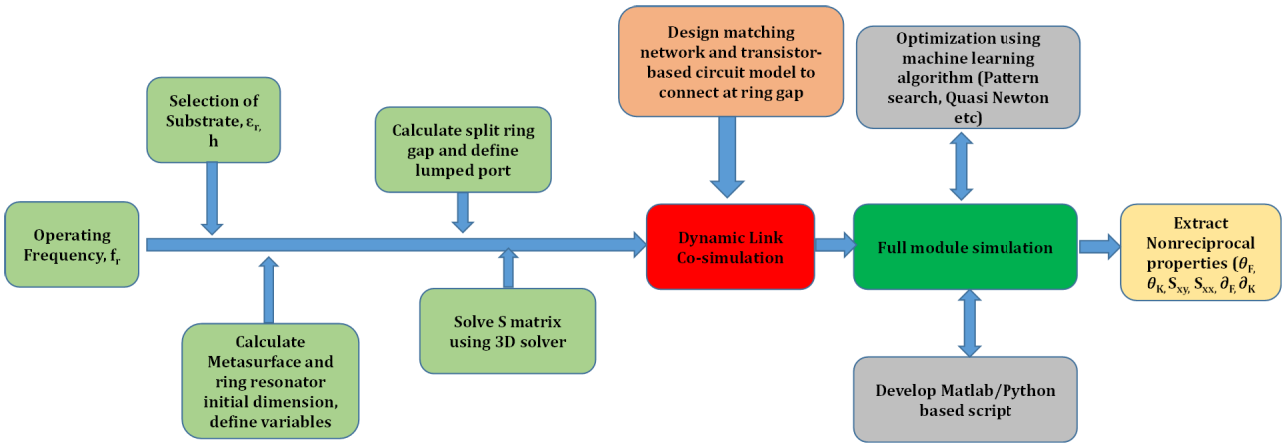

Figure 6. Process flow of the computational approach of the nonreciprocal device design.

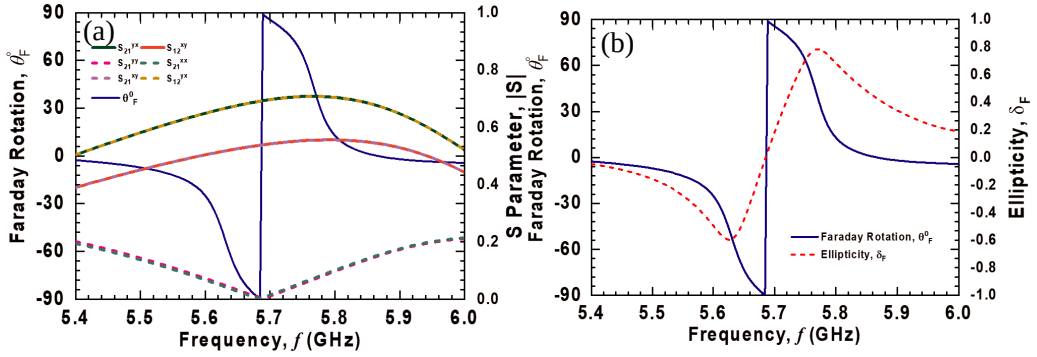

Figure 7. (a) Faraday rotation and scattering parameter over frequency. Co polarized components are same and at resonance those are almost 0. Cross polarized components are different and we observe maximum isolation at resonance. (b) Faraday rotation and ellipticity over frequency.

the signal at region 2. In the time-reversed scenario, the y-polarized wave transmits oppositely, i.e., from antenna 2 to antenna 1, whereas the x-polarized probe (antenna) picks the signal at region 1. For both x-polarized wave and probing, the phases of the transmission coefficients remain the same; therefore, like magnetized ferrites, the co-polarized component does not show any change in phase in the time-reversed situation. However, the cross-polarized components show 180° phase difference at the resonance frequency. This action leads the designed structure to behave like a magnetized ferrite where the permeability tensor has out-of-phase cross-components, evidence of a nonreciprocal gyrotropic response. In Fig. 7(a), the nonreciprocal behavior is evident where we see that the cross-polarized component's magnitude is different, and the resonance magnitude of the co-polarized component is negligible. The design achieved Faraday rotation at resonance at about 90°. Similarly, from Fig. 7(b), at resonance $\delta_F = 0$, i.e., the wave is linear polarized. Fig. 8 shows the Kerr rotation, a reflection-based measurement we can explain as we did for the Faraday rotation. Our previous articles discuss the practical implementation and measurement procedures in detail.

Design steps of a magnet-less nonreciprocal devices such as isolators, circulators, and leaky wave antennas are the same; however, design and optimization to achieve meaningful results are very challenging. For example, impedance and phase matching between circular ring resonator and active/passive component at microwave frequencies are the significant challenges to create artificial non-reciprocity. The excited resonance shows a loss in the presence of mismatch leading to a nonzero standing wave ratio (SWR). The device does not exhibit gyrotropy for an infinite standing wave ratio, hence, nonreciprocity. Therefore, full wave 3D simulation along with optimization cost functions were

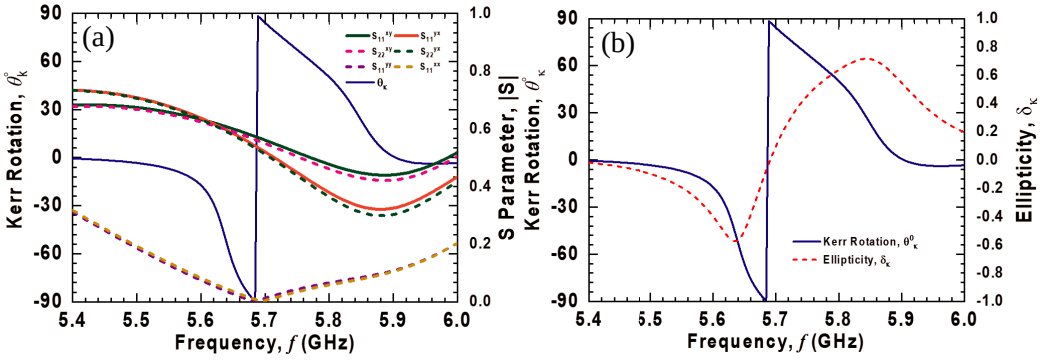

Figure 8. (a) Kerr rotation and scattering parameter over frequency. Co polarized components are same and at resonance those are almost 0. (b) Faraday rotation and ellipticity over frequency.

used in this work and highly recommended for any non-reciprocal device design. Lastly, the number of active/passive components required to implement the artificial gyrotropy can be optimized and reduced. Characterizing nonreciprocal devices is very susceptible where precise bias condition, setup test bench, and careful extraction of data are critical to consider.

6. CONCLUSION

In summary, a detailed computational approach has been presented on a fully electronic non-reciprocal metamaterial. The necessary condition to achieve nonreciprocity, analytical modeling, and steps required for the design have been proposed, discussed, and implemented. With the precision level of engineering, magnet-free non-reciprocal devices can be a possible substitute for conventional ferrite material biased by the permanent magnet in industrial applications such as an isolator, circulator, gyrator, leaky-wave antenna, and 5G applications in the future. We envision that this work's computational approaches will benefit the existing research area of magnet-free non-reciprocal metamaterials.

REFERENCES

1. Cai, W., Y. Fan, Q. Fu, R. Yang, W. Zhu, Y. Zhang, and F. Zhang, "Nonlinearly tunable extraordinary optical transmission in a hybrid metamaterial," *Journal of Physics D: Applied Physics*, Vol. 55, No. 19, 195106, Feb. 2022.
2. Caloz, C., A. Alù, S. Tretyakov, D. Sounas, K. Achouri, and Z.-L. Deck-Léger, "Electromagnetic nonreciprocity," *Physical Review Applied*, Vol. 10, No. 4, 047001, Oct. 2018.
3. Guo, Z., H. Jiang, and H. Chen, "Zero-index and hyperbolic metacavities: Fundamentals and applications," *Journal of Physics D: Applied Physics*, Vol. 55, No. 8, 083001, Oct. 2021.
4. Guo, Z., X. Wu, S. Ke, L. Dong, F. Deng, H. Jiang, and H. Chen, "Rotation controlled topological edge states in a trimer chain composed of meta-atoms," *New Journal of Physics*, Vol. 24, No. 6, 063001, Jun. 2022.
5. Holmes, A. M., M. Sabbaghi, S. Poddar, S. Pakniyat, and G. W. Hanson, "Experimental realization of topologically protected surface magnon polaritons on ceramic YIG ferrites," *2021 International Conference on Electromagnetics in Advanced Applications (ICEAA)*, 204–204, 2021.
6. Kodera, T. and C. Caloz, "Unidirectional loop metamaterials (ULM) as magnetless artificial ferrimagnetic materials: Principles and applications," *IEEE Antennas and Wireless Propagation Letters*, Vol. 17, No. 11, 1943–1947, 2018.
7. Kodera, T., D. Sounas, and C. Caloz, "Magnetless nonreciprocal metamaterial (MNM) technology: Application to microwave components," *IEEE Transactions on Microwave Theory and Techniques*, Vol. 61, 1030–1042, 2013.

8. Kodera, T., D. L. Sounas, and C. Caloz, "Switchable magnetless nonreciprocal metamaterial (MNM) and its application to a switchable faraday rotation metasurface," *IEEE Antennas and Wireless Propagation Letters*, Vol. 11, 1454–1457, 2012.
9. Kodera, T. and C. Caloz, "Unidirectional loop metamaterials (ULM) as magnetless artificial ferrimagnetic materials: Principles and applications," *IEEE Antennas and Wireless Propagation Letters*, Vol. 17, No. 11, 1943–1947, Nov. 2018.
10. Kodera, T., D. L. Sounas, and C. Caloz, "Artificial faraday rotation using a ring metamaterial structure without static magnetic field," *Applied Physics Letters*, Vol. 99, No. 3, 031114, 2011.
11. Kord, A., D. L. Sounas, and A. Alù, "Microwave nonreciprocity," *Proceedings of the IEEE*, Vol. 108, No. 10, 1728–1758, 2020.
12. Landau, L. and E. Lifshitz, "On the theory of the dispersion of magnetic permeability in ferromagnetic bodies," *Phys. Z. Sowjetunion*, Vol. 8, 01, 1992.
13. Lax, B., K. Button, and H. Hagger, "Microwave ferrites and ferrimagnetics," *Physics Today*, Vol. 16, No. 8, 57, 1963.
14. Menzel, C., C. Rockstuhl, and F. Lederer, "Advanced Jones calculus for the classification of periodic metamaterials," *Phys. Rev. A*, Vol. 82, 053811, Nov. 2010.
15. Poddar, S., "Design and analysis of fully-electronic magnet-free non-reciprocal metamaterial," Theses and Dissertations, 2578, 2020, https://dc.uwm.edu/etd/2578.
16. Poddar, S., S. Roy, S. Roy, and Md. T. Hasan, "A dual triangular cut resonator patch antenna for WLAN applications," *2015 International Conference on Electrical Electronic Engineering (ICEEE)*, 237–240, 2015.
17. Polder, D., "VIII. On the theory of ferromagnetic resonance," *The London, Edinburgh, and Dublin Philosophical Magazine and Journal of Science*, Vol. 40, No. 300, 99–115, 1949.
18. Rabus, D. G. and C. Sada, "Ring resonators: Theory and modeling," *Integrated Ring Resonators*, 3–46, Springer International Publishing, Cham, 2020.
19. Roy, S., M. A. Samad, and S. Podder, "Effect of complementary triangular split ring resonator on microstrip patch antenna," *2015 2nd International Conference on Electrical Information and Communication Technologies (EICT)*, 353–358, 2015.
20. Ruesink, F., M.-A. Miri, A. Alù, and E. Verhagen, "Nonreciprocity and magnetic-free isolation based on optomechanical interactions," *Nature Communications*, Vol. 7, No. 1, 13662, Nov. 2016.
21. Xiao, S., T. Wang, T. Liu, C. Zhou, X. Jiang, and J. Zhang, "Active metamaterials and metadevices: A review," *Journal of Physics D: Applied Physics*, Vol. 53, No. 50, 503002, Sep. 2020.